Optimized Spin Crossings and Transition States for Short-range Electron Transfer in Transition Metal Dimers

Marcus Lundberg* and Per E. M. Siegbahn

Department of Physics, Stockholm University, AlbaNova University Center, SE−106 91 Stockholm, Sweden

Received: March 4, 2005; In Final Form: April 5, 2005

Electron-transfer reactions in eight mixed-valence manganese dimers are studied using B3LYP. One of the dimers is a model of the active site of manganese catalase, while another represents a basic building block of the oxygen-evolving complex in photosystem II. The adiabatic reactions are characterized by fully optimized transition states where the single imaginary frequency represents the electron-transfer coordinate. When there is antiferromagnetic coupling between different high-spin centers, electron transfer must be accompanied by a spin transition. Spin transitions are characterized by minimum-energy crossing points between spin surfaces. Three reaction mechanisms have been investigated. First, a single-step reaction where spin flip is concerted with electron transfer. Second, an initial transition to a center with intermediate spin that can be followed by electron transfer. Third, an initial transition to a ferromagnetic state from which the electron can be transferred adiabatically. The complexes prefer the third route with rate-determining barriers ranging from 5.7 kcal/mol to 17.2 kcal/mol for different complexes. The origins of these differences are discussed in terms of oxidation states and ligand environments. Many DFT functionals overestimate charge-transfer interactions, but for the present complexes, the error should be limited because of short Mn−Mn distances.

I. Introduction

Electron-transfer reactions have attracted considerable interest because of their importance in chemistry and biology.[1] In biology, the best known example is the chain of electron-transfer reactions in the photosynthetic reaction center, whose final link on the donor side is the manganese-containing oxygen-evolving complex.[2,3] Any attempt to mimic this important reaction requires good knowledge of the mechanisms of electron transfer.[4]

In the present study, electron-transfer reactions in mixed-valence transition metal dimers[5] are investigated. Many enzymes have active sites that contain at least two transition metals with different oxidation states, i.e., a mixed-valence configuration.[6] One example is manganese catalase that forms a Mn(II,III) dimer during its catalytic cycle, and it has been proposed that further reactivity requires an internal electron transfer to form a Mn(III,II) dimer.[7] This step is shortly described in ref 7, and a further analysis of this reaction is the starting point of the present investigation.

There exists a large number of computational approaches to study electron-transfer reactions; for reviews and some recent examples, see refs 8−14. The rate of thermally activated electron transfer can be described by transition state (TS) theory:

$$k_{ET} = \kappa_{el}\nu_n \exp(-\Delta G^{\ddagger}/k_B T) \quad (1)$$

The reaction barrier ($\Delta G^{\ddagger}$) is the most important factor. If the electron transfer is nonadiabatic, the barrier can be estimated from the reorganization energy (l) and the reaction energy ($\Delta G°$).[1,15] The preexponential factor κ_{el} represents the probability of a successful crossing event, and ν_n is the vibrational frequency along the electron-transfer coordinate.[9,16] In the nonadiabatic case, the preexponential factor can be estimated using, e.g., the Landau−Zener approach, which takes into account the shape of the potential energy surface and the coupling between the two states.

In a short-range adiabatic reaction, there is a large electron-transfer matrix element between the electron donor and the electron acceptor (H_{DA}) that results in a lower value for $\Delta G^{\ddagger}$ compared to that of the corresponding nonadiabatic reaction. The transition state region also becomes more flat, see Figure 1. In the adiabatic limit, the transition probability (κ_{el}) approaches unity and the total preexponential factor becomes $k_B T/h$.

For electron transfer within transition metal dimers, here exemplified by manganese dimers with μ-O or μ-OH bridges, it can be difficult to calculate $\Delta G^{\ddagger}$ in eq 1. One way to estimate the barrier is to calculate λ and H_{DA}. The first problem with this approach is the reorganization energy, i.e., the energy of the electronic structure representing the final state in the geometry of the initial state, see, e.g., ref 17. Because it is not possible to separate the dimer into donor and acceptor parts, it is very difficult to get electronic structures corresponding to the "pure" product because the reactant coordinates represent a heavily distorted geometry. Second, H_{DA} should be evaluated at the transition state and with a complex reaction coordinate; it can be problematic to find a good estimate for the transition state using, e.g., a method of linear extrapolation.[18]

The solution discussed here is a treatment of electron transfer just as any other redox reaction that includes electron transfer as part of a bond breaking/forming process. The DFT functional B3LYP has been used in all investigations because it works well for many other redox reactions and can be applied to rather large systems. In the present examples, the models are small, but the idea is to illustrate a method that can be extended to a large variety of systems. Adiabatic transition states are optimized

* Author to whom correspondence should be addressed. E-mail: marc@physto.se. Telephone: +46−8−55 37 87 06. Fax: +46−8−55 37 86 01.

10.1021/jp051116q CCC: $30.25
Published on Web 04/27/2005

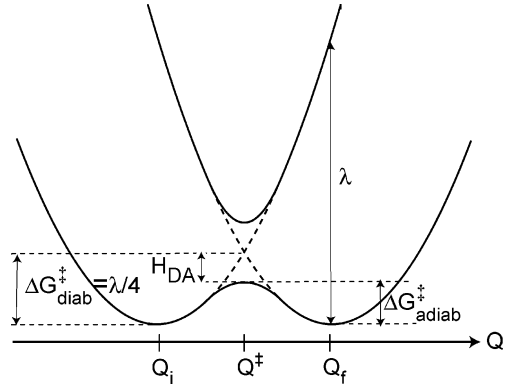

Figure 1. Schematic view of the energetics for a symmetric electron-transfer reaction. Q is the electron-transfer coordinate. For the nonadiabatic case, Marcus theory gives a barrier of $\lambda/4$. In the adiabatic case, the electronic coupling between donor and acceptor causes an avoided crossing at the transition state. A stronger electron-transfer matrix element (H_{DA}) gives a lower barrier with the same reorganization energy λ and a more flat transition state region.

using Hessian matrixes, and $\Delta G^{\ddagger}$ in eq 1 is simply the relative energy between the reactant and the optimized transition state. The Hessian eigenvalue along the reaction coordinate provides information on the shape of the barrier.

A point of the present contribution is to illustrate the importance of spin transitions for electron transfer in antiferromagnetic dimers. The individual manganese centers prefer high spin in the systems studied here. Because the spins of the electrons on the two centers are antiparallel, transfer of an electron from one center to the other requires a change of spin. The spin transitions are estimated to occur on the minimum of the seam where the two spin surfaces cross. If spin−orbit coupling is excluded from the Hamiltonian, the electronic coupling between the two different spin surfaces is zero. These transitions are therefore largely nonadiabatic. The use of seam minima to describe electron transfer has been suggested before.[9,19] To locate spin transitions in transition metal chemistry is not new either, see e.g., refs 20−24, but the present schemes of spin transitions are more diverse than previously described.

Another benefit of the present study is the quantitative comparison of eight manganese dimers with different oxidation states and ligand composition. This analysis enables a quantitative discussion of the factors that affect electron-transfer barriers in manganese dimers.

Regarding quantitative accuracy, it has been noticed that, because of the self-interaction error, most DFT functionals, including B3LYP, seem to overestimate charge-transfer interactions.[25] This is definitely the case for some classical mixed-valence Ru dimers (see below), but it can be argued that the problem should be smaller with μ-O-bridged dimers because of a short metal−metal distance.[26]

The accuracy can therefore still be 3−5 kcal/mol as normally expected for transition metal applications in B3LYP. This is sufficient to distinguish between most reaction pathways and to identify many important effects. No electron transfer rates are reported, only reaction barriers. The first reason is that there are no experimental rates for the present model complexes to compare with. Second, no transition probabilities have been calculated because the effects of the uncertainties in $\Delta G^{\ddagger}$ are expected to dominate over contributions from κ_{el}, especially in the adiabatic limit. The purpose of the present contribution is rather to illustrate the array of reaction mechanisms available for electron transfer than to achieve the best possible match to experimental data.

II. Computational Details

All calculations have been performed with the B3LYP functional[27,28] in an unrestricted formalism. The geometries of the manganese dimers were optimized using the lacvp basis set in Jaguar 5.5.[29] Lacvp is a 6-31G type basis set with effective core potentials (ECPs) for the transition metals.[30] Hessians are calculated using Gaussian03.[31] They are used to optimize transition states and estimate thermal effects and contributions from zero-point vibration. In the present investigation, these effects lower the adiabatic barriers by 1−3 kcal/mol. Final electronic energies are calculated using the lacv3p**+ basis set. This basis set is of triple-ζ quality plus polarization and adds diffuse functions to the heavy atoms.

Solvent effects are important in many charge-transfer reactions.[16,32−35] The present investigation uses a continuum solvent model and assumes equilibrium between polarization and electron transfer. The effects are calculated with the Poisson−Boltzmann solver in Jaguar,[36] and a dielectric constant of 4.0 was chosen to mimic sites inside a low dielectric protein. The solvent radius was set to 1.4 Å. For the present intramolecular reactions, the solvent effects are generally small (<1 kcal/mol).

The energies of the antiferromagnetically coupled states (i.e., low-spin coupled open-shell systems) have been corrected using the broken symmetry approach.[37] In the present investigations, the biggest correction is −0.66 kcal/mol for complex **7** below. Resonance delocalization terms are difficult to estimate correctly, see e.g., ref 38, and are not included in the corrections. This may lead to an underestimation of the spin corrections.

Spin transitions are assumed to occur in the region where the two spin surfaces cross. The computational task is to find the minimum energy on the hypersurface where the two spin states have the same energy.[19,39,40] This is the minimum-energy crossing point (MECP). The MECPs are found with a separate program[40] that extracts gradients from Jaguar B3LYP/lacvp calculations and uses them to construct an effective gradient pointing toward the MECP. The final energies are calculated as outlined above but do not include thermal effects because the MECPs are not stationary points on the potential energy surfaces.

The rate of a spin transition depends both on the height of the crossing point and the size of the manganese spin−orbit coupling matrix element. For transition metal complexes, the height of the crossing point is expected to be strongly dominating. The effect of the spin−orbit coupling on the barrier itself is expected to be small, and when it comes to the transition probability, even a poor spin−orbit coupling is not expected to slow the reaction by more than a factor of 10−100. This would correspond to an upward shift of the crossing point by only 2 kcal/mol. Because this is within the error bars of the B3LYP functional, the effect of spin−orbit coupling has been neglected in the present study.

III. Results and Discussions

In the present section, two examples with very different electron-transfer characteristics are first discussed. The first example is a neutral Mn(II,III) dimer with bridging μ-OH ligands (complex **1**). This is a model of the active site in manganese catalase adopted from ref 7 and has water, formate, and ammonia ligands (see Figure 2). The second example is a negatively charged Mn(III,IV) dimer with bridging μ-O ligands (complex **2**). This complex has only water-based ligands, OH, and H_2O (see Figure 3). There is no direct biological precursor for this model, but a Mn(III,IV) dimer with μ-O bridges is a

TABLE 1: Distances and Mulliken Spin Populations of Important Stationary Points for Electron Transfer in Complex 1[a]

	distance to Mn1 (Å)							distance to Mn2 (Å)					Mulliken spin	
state	Mn2	O3	O4	O8	N9	O10	O11	O3	O4	O5	O6	O7	Mn1	Mn2
reactant	3.10	2.15	2.29	2.27	2.28	2.14	2.17	1.84	1.90	1.92	2.10	2.13	4.82	−3.86
TS A	3.01	1.95	2.11	2.24	2.17	2.05	2.33	1.95	2.03	2.01	2.18	2.12	4.74	−3.87
TS AF	3.12	2.15	2.28	2.28	2.27	2.14	2.17	1.85	1.91	1.92	2.11	2.12	4.83	−3.80
ferro	3.11	2.14	2.29	2.26	2.27	2.14	2.19	1.85	1.91	1.92	2.11	2.12	4.82	3.86
TS C	3.08	1.95	2.08	2.26	2.16	2.03	2.23	1.97	2.04	2.01	2.19	2.12	4.41	4.49
product	3.05	1.84	1.98	2.24	2.09	1.96	2.26	2.09	2.16	2.10	2.24	2.11	−3.84	4.79

[a] Atomic labels are shown in Figure 2 and positions in the potential energy diagrams are shown in Figures 4−6.

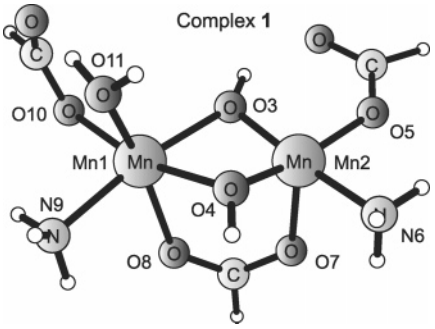

Figure 2. Mn(II,III) dimer $[(HCO_2)(NH_3)(H_2O)Mn(\mu\text{-}OH)_2(\mu\text{-}O_2CH)\text{-}Mn(O_2CH)(NH_3)]$ used as a model of the active site of manganese catalase (complex **1**). Mn−ligand distances and Mulliken spin populations for all stationary points are reported in Table 1.

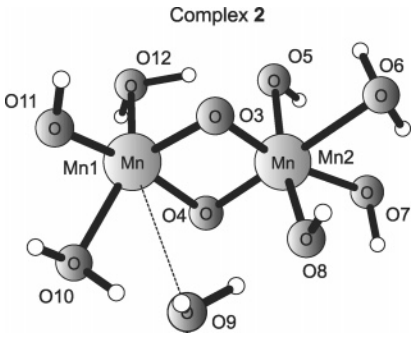

Figure 3. Mn(III,IV) dimer with water-based ligands $[(H_2O)(OH)_3\text{-}Mn(\mu\text{-}O)_2Mn(OH)_3(H_2O)]^-$ (complex **2**), model of a basic building block in the oxygen-evolving complex in photosystem II. Mn−ligand distances and Mulliken spin populations for all stationary points are reported in Table 2.

basic building block of the oxygen-evolving complex in photosystem II. The oxygen-evolving complex transfers electrons to a tyrosyl radical (Tyr_z). These steps may require that the electrons are first transferred to a suitable position in the manganese cluster. Published X-ray structures of photosystem II[41−43] assigns amino acids to less than half of the manganese binding sites, and unassigned positions are likely to be occupied by H_2O or OH ligands.[44] Effects of Glu and Asp ligands can be estimated by adding carboxylate groups, see complexes **4** and **7** below.

In the ground state of complex **1**, the six-coordinated manganese to the left (Mn1) has a spin of 4.82 (Mn(II), five d-electrons, high spin), while the five-coordinated manganese to the right (Mn2) has a spin of −3.86 (Mn(III), four d-electrons, high spin). The two centers are antiferromagnetically coupled. Spin populations and Mn−ligand distances for the important structures along the reaction pathways of complex **1** are shown in Table 1. The cost of moving the electron to the right side (ΔG_0) is 3.7 kcal/mol, see Figure 4. Because of the antiferromagnetic coupling of two high-spin centers, three distinct alternatives for this electron transfer can be imagined, but all

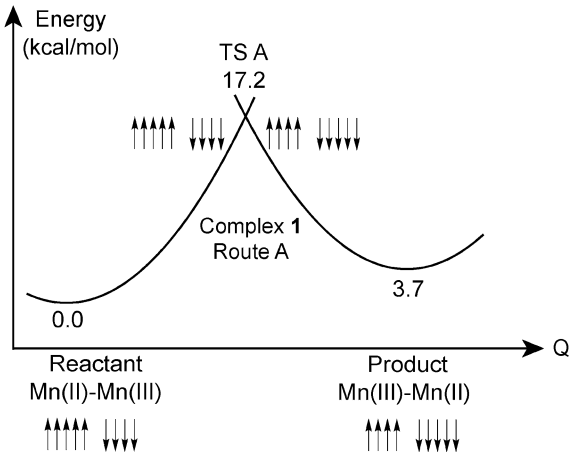

Figure 4. Potential energy diagram for electron transfer from Mn_2-(II,III) to Mn_2(III,II) in complex **1** using route A. This is a single-step reaction where electron transfer is concerted with spin transition.

of them include at least one spin transition. Without spin transition, the transferred electron would become antiparallel to the other electrons on the accepting metal center and this is not a stable state.

Route A is a single-step reaction where the electron transfer is concerted with a spin transition. Computationally, the transition state is the minimum energy crossing point (MECP) between the reactant doublet state (antiferromagnetic Mn(II,-III)) and the product doublet state (antiferromagnetic Mn(III,-II)). This spin crossing is located 17.2 kcal/mol above the reactant, see Figure 4. Judging from the spin populations of the reactant state at the crossing point (4.74, −3.87), the electron remains on the first manganese until the spin transition occurs. In this description, the reaction is nonadiabatic.

Route B is a two-step process (see Figure 5). It starts with a change of spin for one of the five electrons on Mn(II) to create a Mn(II) center with four spins up and one down ($S = 3/2$). From this state, the antiparallel electron can easily be transferred to the other manganese. The initial intermediate spin state lies approximately 30 kcal/mol above the reactant but is difficult to fully converge because, from this point, the barrier for electron transfer seems to be almost negligible. This reaction path is better described for complex **2**, but the high-energy intermediate structure shows that this route is not important. There is, of course, a corresponding route where the electron is first transferred to the acceptor side and then changes its spin, but it is very similar to the one previously described. The energy of an intermediate spin Mn(II) on the right side is 33 kcal/mol.

The third route, route C, is more similar to the adiabatic reactions normally outlined for electron transfer but has two additional steps. The problem with antiparallel alignment of electrons on different centers can be avoided by first making the transition to a ferromagnetic state. For complex **1**, the splitting between the antiferromagnetic doublet state and the

TABLE 2: Distances and Mulliken Spin Populations of Important Stationary Points for Electron Transfer in Complex 2[a]

	distance to Mn1 (Å)							distance to Mn2 (Å)						Mulliken spin	
state	Mn2	O3	O4	O9	O10	O11	O12	O3	O4	O5	O6	O7	O8	Mn1	Mn2
reactant	2.72	1.85	1.90	3.23	2.10	1.87	2.25	1.83	1.78	1.95	2.23	1.96	1.93	3.82	−2.81
TS A	2.69	1.83	1.84	2.02	2.25	1.90	2.18	1.84	1.83	2.02	2.25	1.90	2.18	3.71	−2.68
TS B	2.61	1.81	1.96	1.98	2.12	1.95	1.91	1.84	1.75	1.99	2.26	1.93	1.95	3.75	−2.62
INT B	2.65	1.83	1.93	2.05	2.15	1.96	2.02	1.84	1.76	1.97	2.24	1.94	1.96	−1.96	2.78
TS AF	2.79	1.97	1.79	3.42	2.09	1.86	2.15	1.84	1.97	2.00	2.49	1.92	1.93	3.75	−3.09
ferro	2.72	1.85	1.90	3.18	2.10	1.87	2.26	1.84	1.78	1.95	2.24	1.95	1.93	3.81	2.91
TS C	2.70	1.89	1.82	1.99	2.39	1.90	2.17	1.82	1.89	1.99	2.39	1.90	2.17	3.53	3.45
product	2.72	1.78	1.83	1.95	2.23	1.96	1.93	1.90	1.85	3.23	2.10	1.87	2.25	−2.81	3.82

[a] Atomic labels are shown in Figure 3 and positions in the potential energy diagrams are shown in Figures 7, 9, and 10.

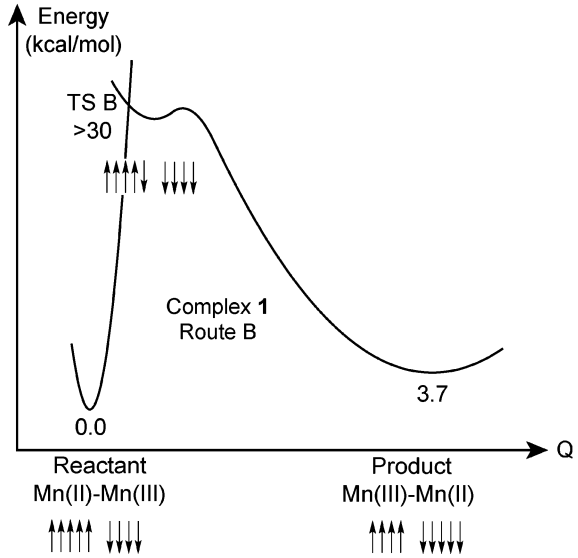

Figure 5. Potential energy diagram for electron transfer from Mn_2-(II,III) to Mn_2(III,II) in complex **1** using route B. This is a two-step process where a spin transition to an intermediate spin ($S = 3/2$) state on Mn(II) precedes electron transfer.

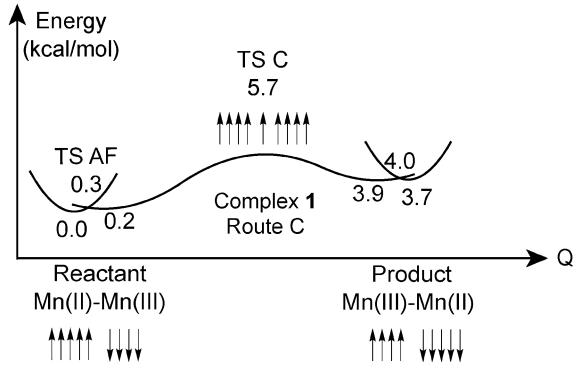

Figure 6. Potential energy diagram for electron transfer from Mn_2-(II,III) to Mn_2(III,II) in complex **1** using route C. This route includes a transfer to a ferromagnetic state (TS AF), followed by adiabatic electron transfer (TS C), and finally, a transition back to an antiferromagnetic state.

ferromagnetic state (multiplicity 10) is small (0.2 kcal/mol). The crossing between the two states is located at 0.3 kcal/mol, and the geometry of the crossing point is very similar to the geometry of the ferromagnetic state. From the ferromagnetic state, a transition state for electron transfer can be optimized, and the total barrier is 5.7 kcal/mol, see Figure 6. At the transition state, the electron is almost equally divided between the two centers which now have spin populations of 4.41 and 4.49. The imaginary frequency for this transition state is 237i cm^{-1}, and it shows concerted changes in Mn−ligand distances.

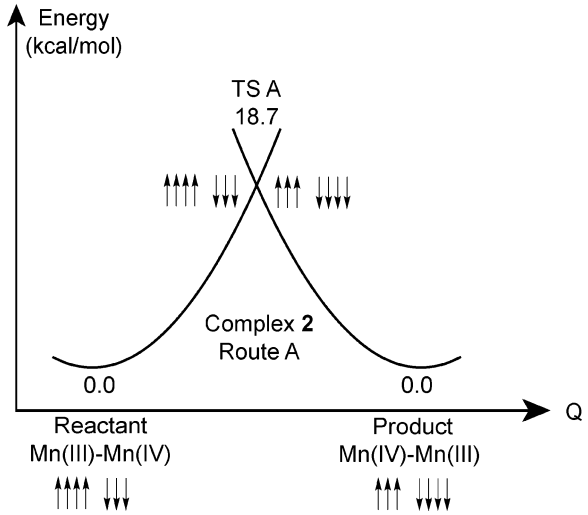

Figure 7. Potential energy diagram for electron transfer from Mn_2-(III,IV) to Mn_2(IV,III) in complex **2** using route A. This is a single-step reaction where electron transfer is concerted with spin transition.

The final third step is the transition back to the antiferromagnetic product state. Counted from the ferromagnetic state, the barrier is very small, on the order of 0.1 kcal/mol.

In total, the system prefers route C where all three transition states have very low barriers, the highest being 5.7 kcal/mol for the electron-transfer step. Using eq 1 in the adiabatic limit, the reaction occurs in nanoseconds and does not have any effect on the rate of the enzymatic reaction.

A different behavior, and much higher barriers, is encountered for complex **2**. This is the Mn(III,IV) dimer with μ-O bridges and water-based ligands shown in Figure 3. In this particular system, reactant and product states are degenerate and connected by C_i symmetry. In the ground state of complex **2**, the manganese to the left (Mn1) has a spin of 3.82 (Mn(III), four d-electrons, high spin) while the manganese to the right (Mn2) has a spin of −2.81 (Mn(IV), three d-electrons, high spin). The centers are antiferromagnetically coupled. The primary geometric difference between the Mn(III) ion and the Mn(IV) ion is that the former has a clear Jahn−Teller axis cis to the μ-O bridges with one water molecule that is hardly bound at all (bond distance of 3.2 Å), see Figure 3. Spin populations and Mn−ligand distances for the important structures along the reaction pathways of complex **2** are shown in Table 2.

The three different mechanisms outlined for complex **1** above are investigated. In route A, where the spin transition is concerted with an electron transfer, the MECP is located at 18.7 kcal/mol, see Figure 7. As expected, the main reaction coordinate is the change in ligands cis to the μ-O bridges. The reactant has two water ligands, O9 and O12, along this axis, 3.23 and 2.25 Å from the Mn(III) ion, respectively. These ligand distances change to 2.02 and 2.18 Å, respectively, when the spin crossing

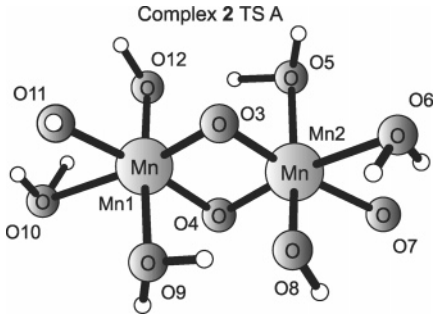

Figure 8. Geometry of the MECP between an antiferromagnetic Mn_2-(III,IV) state and an antiferromagnetic Mn_2(IV,III) state in complex **2**. Mn−ligand distances and Mulliken spin populations are reported in Table 2.

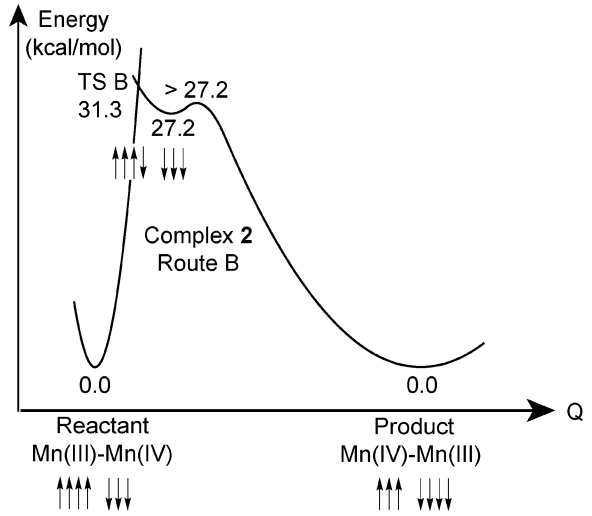

Figure 9. Potential energy diagram for electron transfer from Mn_2-(III,IV) to Mn_2(IV,III) in complex **2** using route B. This is a two-step process where a spin transition to an intermediate spin ($S = 1$) state on Mn(III) precedes electron transfer.

is reached. The shorter distance belongs to a hydroxo ligand that is formed by a loss of a proton to a ligand on the other manganese. This proton transfer is completed before the spin crossing is reached. The geometry of the MECP is shown in Figure 8. The electrons remain localized with spin populations of 3.71 and −2.68 on the two manganese until the spin transition occurs.

In route B, the spin crossing that leads from the high-spin Mn(III) ($S = 2$) to the intermediate spin Mn(III) ($S = 1$) has been optimized. It is located 31.3 kcal/mol above the reactant, and the resulting intermediate structure lies at 27.2 kcal/mol. The potential energy diagram for this route is shown in Figure 9. In the spin crossing, the Mn−Mn distance is very short (2.61 Å), and several Mn−ligand distances have changed compared to that of the reactant structure, see Table 2. The barrier for further electron transfer has not been investigated because the energy of the intermediate structure is higher than that of the transition state in route A.

Continuing with route C, the crossing from an antiferro- to a ferromagnetic state has a barrier of 10.9 kcal/mol, see Figure 10. This step is rarely, if ever, discussed but does apparently have a substantial barrier in some complexes. To reach the spin crossing and eliminate the 3.2 kcal/mol splitting between the two states, the distance between the two manganese increases from 2.72 to 2.79 Å. The spin on the Mn(IV) ion (Mn2) increases from 2.78 to 3.09 on the antiferromagnetic surface (and to 3.28 on the ferromagnetic one). At the same time, the

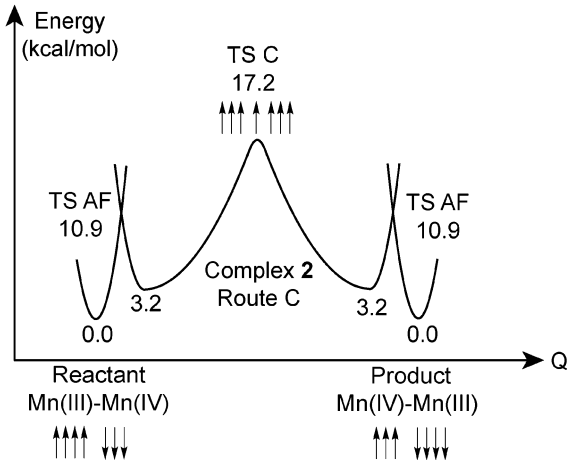

Figure 10. Potential energy diagram for electron transfer from Mn_2-(III,IV) to Mn_2(IV,III) in complex **2** using route C. This route includes a transfer to a ferromagnetic state (TS AF), followed by adiabatic electron transfer (TS C), and finally a transition back to an antiferromagnetic state.

Mn2−O4 ligand distance increases from 1.78 to 1.97 Å (see Figure 8 for atomic labels). Together, these observations indicate that the transition requires that some Mn(III) character is transferred to the center that is initially Mn(IV).

From the ferromagnetic intermediate, three different methods can be employed to find the adiabatic transition state for electron transfer. Many electron-transfer systems exhibit some sort of symmetry between initial and final states,[5] and this symmetry can be used to locate a transition state. In complex **2**, initial and final states are connected by C_i symmetry, and a C_i symmetric structure will thus be encountered between reactant and product. This structure is a maximum on the energy surface if the reaction has an odd number of steps, otherwise it is a minimum. In the present single-step reaction, a constrained optimization where the C_i symmetry is maintained thus leads directly to a transition state. For this model, the transition state is found at 17.2 kcal/mol. The spins of the manganese are 3.53 and 3.45, not exactly equal as would be expected from a symmetric transition state. This is the result of an orbital symmetry breaking of the C_i state. The difference in spin can be decreased with a tighter geometry convergence criteria but the change in energy is small. Mn−ligand distances in the transition state are shown in Table 2.

A second alternative is to guess the structure of the transition state, calculate a Hessian at this point, and use this information to find the real transition state. This is the method employed for complex **1**. For the present complex, the previous optimization had already provided a transition state structure, and a Hessian calculation, without any constraints, was performed to confirm that the previous procedure really did lead to a transition state. The calculated Hessian has a single imaginary frequency of 1880i cm^{-1} and the forces are very low, thus confirming the TS character of this structure. The higher frequency compared to that of the previous Mn(II,III) complex (237i cm^{-1}) is due to a force constant that is 150 times higher for the Mn(III,IV) complex. This indicates a very sharp transition and a rather small electron-transfer matrix element.

After symmetry constraints and Hessians, the third alternative to locate the transition state is to optimize the "pseudo" crossing between reactant and product states. This is possible because the C_i symmetric geometries exhibit orbital symmetry breaking. To find a reasonable starting geometry for the optimization that is different from the previously located transition state, an

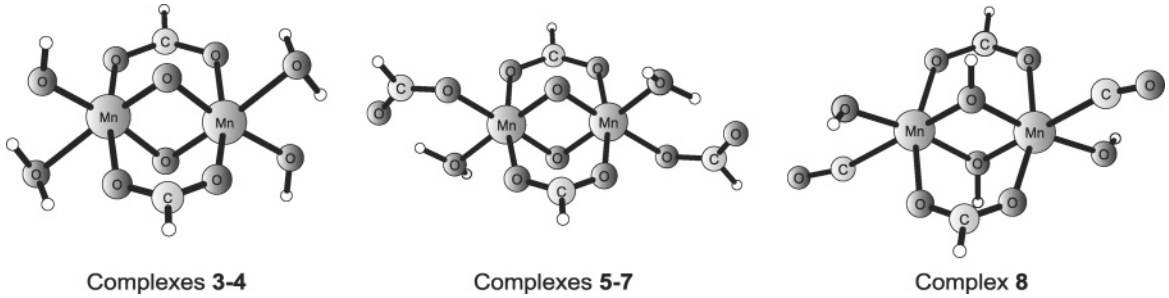

Figure 11. Three ligand types are used to construct the six complexes **3**−**8** using different oxidation states and bridging ligands (μ-oxo or μ-hydroxo). From left to right are the complexes: $[(H_2O)(OH)Mn(\mu\text{-}O)_2(\mu\text{-}O_2CH)_2Mn(OH)(H_2O)]^-$, $[(H_2O)(HCO_2)Mn(\mu\text{-}O)_2(\mu\text{-}O_2CH)_2Mn(HCO_2)(H_2O)]^-$, and $[(OH)(HCO_2)Mn(\mu\text{-}OH)_2(\mu\text{-}O_2CH)_2Mn(HCO_2)(OH)]^-$. All complexes, including their oxidation states and bridging ligands, are listed in Table 3.

TABLE 3: Energy Barriers for Electron Transfer in the Complexes 1−8 for the Routes A, B, and C.

no.	charge	oxidation state	bridging ligands	TS A (kcal/mol)	TS B (kcal/mol)	ΔE(A−F) (kcal/mol)	TS AF (kcal/mol)	TS C (kcal/mol)	TS frequency (cm^{-1})
1	0	(II,III)	$(\mu\text{-OH})_2$	17.2	>30	0.2	0.3	5.7	−237i
2	−1	(III,IV)	$(\mu\text{-O})_2$	18.7	31.3	3.2	10.9	17.2	−1880i
3	−1	(II,III)	$(\mu\text{-OH})_2$	22.4	>35	0.8	2.8	13.3	−335i
4	−1	(III,IV)	$(\mu\text{-O})_2$	16.7	>24.5	3.3	6.2	15.7	−2740i
5	−1	(II,III)	$(\mu\text{-OH})_2$	21.6	>32	0.7	1.3	11.8	−334i
6	+1	(III,IV)	$(\mu\text{-OH})_2$	14.2	>20	0.1	0.2	8.2	−983i
7	−1	(III,IV)	$(\mu\text{-O})_2$	13.0	>20[b]	3.3	12.4	12.8	−1148i
8	−1	(II,III)	$(\mu\text{-OH})_2$	13.6	>32[c]	1.1	2.3	6.4	−313i

[a] For route B, the energy of the state with intermediate spin (Mn(III) with $S = 3/2$ or Mn(IV) with $S = 1$) has in many cases been taken as an approximate TS barrier. ΔE(A−F) is the energy difference between the antiferromagnetic and the ferromagnetic states and TS AF is the energy barrier for a transition between these two states. Complex **1** is shown in Figure 2, complex **2** in Figure 3, and complexes **3**−**8** in Figure 4. [b] Not converged, estimated from complex **6**. [c] Not converged, estimated from complex **5**.

optimization was performed where *both* orbitals and geometry were constrained to C_i symmetry. From this geometry, the nonsymmetric densities are found by using the reactant and product orbitals as starting guesses. The two resulting electronic states have manganese spin populations of 3.74−3.17 and 3.17−3.74 and they are degenerate, of course. This geometry is a crossing point between reactant and product states but it is not a minimum on that hypersurface. The true transition state can be reached by optimizing the minimum energy crossing point between these two states. The result is a geometry very similar to the previously optimized transition state. The energy difference between the two methods is 0.1 kcal/mol, and the main geometric difference is that the water ligands O6 and O10 change their distances to manganese by 0.08 Å. In general, the energy is not very sensitive to the exact length of these long Mn−water distances. The final spins are 3.53−3.44 (and 3.45−3.53 on the other surface), and the difference is again attributed to limited geometry convergence. This is a "pseudo" crossing because both states exist on the same potential energy surface. It is the limited convergence that keeps the algorithm from ending up in two states that are identical.

After passing the TS at 17.2 kcal/mol, the dimer should go back to the antiferromagnetic state. Because of symmetry, this step is identical to the first spin transition in route C, which has a barrier of 10.9 kcal/mol.

In total, the energy difference between the transition states of route A (18.7 kcal/mol) and route C (17.2 kcal/mol) is within the accuracy of the present method. It should also be noted that the barriers cannot be accurately compared because with these small energy differences, contributions from spin−orbit coupling, barrier shape, and thermal effects can have some influence on the final results. It is therefore difficult to assign which of the two routes would be preferred for complex **2**.

In the introduction, the problems of calculating the reorganization energy were discussed. In this specific case, it should be the energy of a Mn(III,IV) density in a Mn(IV,III) geometry. This density is very difficult to converge, but it happened to be possible using the antiferromagnetic state and the lacvp basis set. However, the manganese spin populations are only 3.40 and −2.34, (compared to the expected 3.8 and −2.8), which indicates that this is not a pure Mn(III,IV) state after all. The relative energy of this metastable state (i.e., the reorganization energy) is 55.1 kcal/mol and the barrier for a nonadiabatic crossing ($\Delta G^{\ddagger}$) is 13.8 kcal/mol ($\lambda/4$). This value should be compared to the calculated spin crossing for route A, which is 17.8 kcal/mol using the lacvp basis set. The main cause of the 4 kcal/mol deviation is probably that the converged Mn(III,IV)-type state has a lower energy than a pure state would have had.

The electron-transfer barriers for the complexes **1** and **2** differ by 11.5 kcal/mol, corresponding to a rate difference by a factor of 10^8. The shapes of the transition states are also very different, as judged by the magnitude of the second derivatives (factor of 150). To understand the origins of these differences, transition states for electron-transfer reactions using routes A−C were calculated for six other model manganese dimers, see Figure 11. The two main variables are the oxidation state, (II,III) or (III,IV), and the ligand environment. The ligands of the new complexes are related to complex **2** but designed to gradually minimize the number of hydrogen bonding possibilities and lower the reorganization energy. To facilitate the location of transition states, all these complexes exhibit C_i symmetry between reactant and product.

Results for all routes in all complexes are summarized in Table 3. Because route B tends to give high barriers, only the energy of the intermediate structure has been calculated, and this energy is consistently higher than the transition states of the other routes.

The complexes in the (II,III) oxidation state (**1**, **3**, **5**, and **8**) prefer the adiabatic route C over the nonadiabatic route A by 7−12 kcal/mol, see Table 3. It is tempting to assign the difference in barrier height between mechanisms A and C to

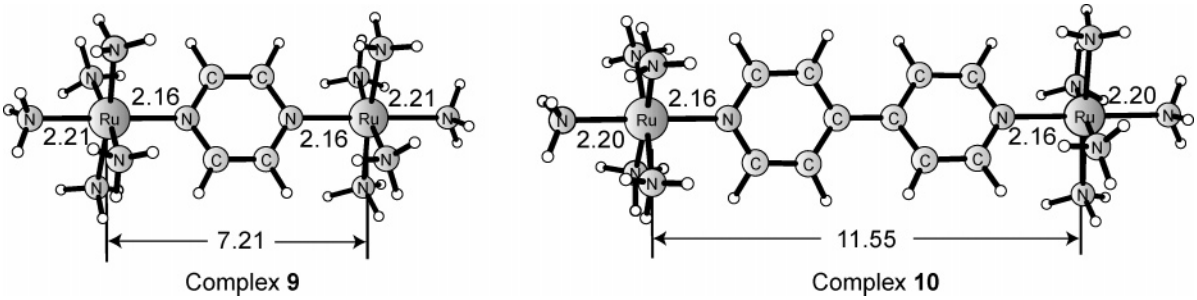

Figure 12. Two ruthenium charge-transfer complexes with a single unpaired electron. Labels show distances in Å. B3LYP predicts delocalized states for both of them with spin populations of 0.66−0.66 for complex **9** and 0.54−0.54 for complex **10**. No barriers for electron transfer can be detected. Experimentally, at least complex **10** is known to localize.

the electron-transfer matrix element, but this is not perfectly correct. Transition state geometries are different and energy barriers are not calculated in exactly the same way. Transition states in route C are stabilized by thermal effects of 1−3 kcal/mol. These effects have not been calculated for the spin crossings in route A because they are not stationary points on the potential energy surfaces. The barrier for route C also includes the coupling between antiferro- and ferromagnetic states.

The transition state barriers for the adiabatic route C range from 5.7 to 13.7 kcal/mol, and this span is partly due to a difference in reorganization energy. This difference is most clearly seen by comparing complexes **3** and **8** in Table 3. For these two complexes, the effect of the reorganization energy on the barrier differs by 7 kcal/mol.

The complexes in the (III,IV) oxidation state with μ-O bridges all have similar TS barriers for routes A and C. Because the barrier for the adiabatic route C is lowered by the electronic coupling, it seems reasonable that it should be lower than that for the nonadiabatic route A that does not include any coupling. However, the two mechanisms proceed along different reaction paths. In addition, the energy difference between the antiferromagnetic and the ferromagnetic state must be added to TS C. The relation between the increase in barrier from the antiferromagnetic coupling and the decrease in barrier from the electron-transfer matrix element may vary. With the present accuracy and the neglect of the different transition probabilities for the transition states A and C, it is difficult to determine which route would be preferred.

In any case, the electron-transfer matrix element is much smaller for the (III,IV) complexes with μ-O bridges than that in the (II,III) complexes with μ-OH bridges. This conclusion is supported by the narrow transition states for the (III,IV) complexes as judged by the magnitude of the imaginary frequencies (all $>1100i$ cm^{-1}, see Table 3). For the (II,III) complexes with μ-OH bridges, the corresponding imaginary frequencies are <350 cm^{-1}. It is interesting to note that the (II,III) complexes have relatively strong electronic-coupling matrix elements but small energy differences between antiferro- and ferromagnetic states.

To see whether the differences in electronic coupling between (II,III) complexes with μ-OH bridges and (III,IV) complexes with μ-O bridges depend on the oxidation state or the bridging ligands, a single (III,IV) complex with μ-OH bridges (complex **6**) was investigated. In this complex, the adiabatic route C is preferred by 6.0 kcal/mol This result is between the results for (II,III) and (III,IV) complexes. The imaginary frequency is 986 cm^{-1}, which is also between the two groups, even though it is rather close to the related (III,IV) complex **7**. On the basis of this single example, the μ-OH bridges cannot explain the entire difference between (II,III) and (III,IV) complexes, but they do seem to stabilize the adiabatic transition state by a few kcal/mol.

Comparing complexes with the same ligands but different oxidation states, e.g., **3** to **4** and **5** to **7**, the reorganization energies are higher for the (II,III) complexes. This is mainly due to the possibilities of hydrogen bonding to the μ-OH ligands that leads to larger rearrangements. All barriers are calculated from the minimum that is reached by releasing the transition state. Other stable structures could possibly be found by enforcing larger rearrangements of the ligands, but this has not been investigated.

The height of the barrier that is passed in the transition from an antiferromagnetic to a ferromagnetic state is related to the splitting between the two states. The highest barrier detected is 12.4 kcal/mol for complex **7**. This is actually very similar to the other barriers for electron transfer in this complex (13.0 and 12.8 kcal/mol). It is a rather surprising result that a change of coupling between two manganese centers could possibly be the rate-limiting step in an electron-transfer reaction, even though the splitting between the states is rather small.

After the investigation of the model manganese complexes, the idea was to test the method on some well-characterized mixed-valence Ru(II,III) dimers. The Ru complexes have low spin on individual centers, and electron transfer does not require any change of spin. This removes many of the complexities described for the manganese complexes above. Results for two complexes are reported, the Creutz−Taube complex decaammine(μ-pyrazine)diruthenium(5+) (complex **9**) and the related decaammine(μ-4,4′-bipyridine)diruthenium(5+) (complex **10**), see Figure 12. For the Creutz−Taube complex, there is still a debate as to whether there is a barrier for electron transfer or not, see, e.g., ref 5, but the other complex (**10**) is known to be at least partly localized[45] and should have a barrier for electron transfer. These two complexes have previously been investigated with different theoretical methods, see, e.g., refs 46−50. When applied, DFT predicts complete delocalization,[48,49] while, e.g., HF, predicts a more localized state.[49] This is in line with previous observations that DFT functionals seem to overestimate the charge-transfer interactions in many complexes.[25]

As could be expected from previous attempts using DFT, the present calculations do not give any barriers for electron transfer in either complex **9** or complex **10**. In both cases, the unpaired electron is totally delocalized between the two centers in the ground state. At least for complex **10**, this is contrary to experimental evidence. These problems with B3LYP may raise some questions concerning the accuracy of the calculated barriers in the manganese complexes above. However, if the errors are due to the effects of the self-interaction error, it is unlikely that the transition states of the manganese dimers are

significantly affected. The Mn−Mn distances are 2.7−3.0 Å, while the Ru−Ru distances in the two complexes above are 7−12 Å, and the effect of the self-interaction error should increase with increasing metal−metal distance.[26] Still, it should be valuable to apply self-interaction corrected functionals to the present problems. Many interesting metalloorganic complexes have long metal−metal distances that prevent the use of many DFT functionals in the way outlined here.

IV. Conclusion

Electron transfer reactions are normally described by the reorganization energy (λ) and the electron-transfer matrix element between donor and acceptor at the transition state (H_{DA}). In some transition metal systems, these variables are difficult to calculate because of complex reaction coordinates and a plethora of electronic states. The present contribution treats electron transfer as any other redox reaction and calculates electron transfer barriers directly from transition states optimized using Hessian matrixes.

Among the complexes investigated is a model of the active site of manganese catalase. The barrier for electron transfer is estimated to be only 5.7 kcal/mol, and such a fast electron-transfer step should not have any effect on the kinetics of the enzyme.

In manganese dimers, the two centers couple antiferromagnetically, and electrons on different centers have antiparallel spins. Electron transfer must therefore be accompanied by a change of spin. Three mechanisms of electron transfer have been investigated, and they all contain interesting spin crossings. Route A is a nonadiabatic single-step reaction where the spin transition is concerted with electron transfer. Route B requires an initial transition to an intermediate spin state on one center. In one of the complexes, the barrier for this transition from high-spin Mn(III) ($S = 2$) to intermediate-spin Mn(III) ($S = 1$) lies 4.1 kcal/mol above the $S = 1$ Mn(III) state. After that transition, the antiparallel electron can be transferred to the second center. Route C goes through an initial transition to a ferromagnetic state where the electron transfer can occur adiabatically. The barrier for switching between antiferromagnetic and ferromagnetic state is related to the strength of the coupling. In a (III,-IV) complex with a ferro- to antiferromagnetic splitting of 3.3 kcal/mol, the barrier is as high as 12.4 kcal/mol.

The Mn(II,III) dimers prefer the adiabatic route C because of a relatively strong electron-transfer matrix element. For Mn-(III,IV) complexes, the electron-transfer matrix element is smaller and the transition states for routes A and C are close in energy.

It has been noticed that, because of the self-interaction error, most DFT functionals overestimate charge-transfer interactions. This leads to too-low barriers for electron transfer in complexes with medium and long metal−metal distances. This prevents a good description of the well-known mixed-valence Ru dimers but probably has no significant effect on the transition states of the presently investigated manganese dimers because the Mn−Mn distances are so short.

Acknowledgment. We would like to thank Dr J. N. Harvey for providing us with a copy of his MECP program.

References and Notes

(1) Marcus R. A. *Rev. Mod. Phys.* **1993**, *65*, 599.
(2) Tommos, C.; Babcock, G. T. *Biochim. Biophys. Acta* **2000**, *1458*, 199.
(3) Renger, G. *Biochim. Biophys. Acta* **2001**, *1503*, 210.
(4) Sjödin, M.; Styring, S.; Åkermark, B.; Sun, L.; Hammarström, L. *J. Am. Chem. Soc.* **2000**, *122*, 3932.
(5) Demadis, K. D.; Hartshorn, C. M.; Meyer, T. J. *Chem. Rev.* **2001**, *101*, 2655.
(6) Siegbahn, P. E. M. *Q. Rev. Biophys.* **2003**, *36*, 91.
(7) Siegbahn, P. E. M. *Theor. Chem. Acc.* **2001**, *105*, 197.
(8) Newton, M. D.; Sutin, N. *Annu. Rev. Phys. Chem.* **1984**, *35*, 437.
(9) Newton, M. D. *Chem. Rev.* **1991**, *91*, 767.
(10) Amini, A.; Harriman, A. *J. Photochem. Photobiol., C* **2003**, *4*, 155.
(11) Rosso, K. M.; Smith, D. M. A.; Dupuis, D. *J. Phys. Chem. A* **2004**, *108*, 5242.
(12) You, Z.-Q.; Shao, Y.; Hsu, C.-P. *Chem. Phys. Lett.* **2004**, *390*, 116.
(13) Lu, S.-Z.; Li, X.-Y.; Liu, J. F. *J. Phys. Chem. A* **2004**, *108*, 4125.
(14) Sim, E. *J. Phys. Chem. B* **2004**, *108*, 19093.
(15) Marcus, R. A. *J. Chem. Phys.* **1965**, *43*, 679.
(16) Chen, P.; Meyer, T. J. *Chem. Rev.* **1998**, *98*, 1439.
(17) Klimkans, A.; Larsson, S. *Chem. Phys.* **1994**, *189*, 25.
(18) Farazdel, A.; Dupuis, M.; Clementi, E.; Aviram, A. *J. Am. Chem. Soc.* **1990**, *112*, 4206.
(19) Koga, N.; Morokuma, K. *Chem. Phys. Lett.* **1985**, *119*, 371.
(20) Smith, K. M.; Poli, R.; Harvey, J. N. *Chem.—Eur. J.* **2001**, *7*, 1679.
(21) Hess, J. S.; Leelasubcharoen, S.; Rheingold, A. L.; Doren, D. J.; Theopold, K. H. *J. Am. Chem. Soc.* **2002**, *124*, 2454.
(22) Jensen, V. R.; Poli, R. *J. Phys. Chem. A* **2003**, *107*, 1424.
(23) Carreón, J.-L.; Harvey, J. N. *J. Am. Chem. Soc.* **2004**, *126*, 5789.
(24) Lundberg, M.; Siegbahn, P. E. M. *Chem. Phys. Lett.* **2005**, *401*, 347.
(25) Ruiz, E.; Salahub, D. R.; Vela, A. *J. Phys. Chem.* **1996**, *100*, 12265.
(26) Lundberg, M.; Siegbahn, P. E. M. Submitted.
(27) Becke, A. D. *J. Chem. Phys.* **1993**, *98*, 1372.
(28) Becke, A. D. *J. Chem. Phys.* **1993**, *98*, 5648.
(29) *Jaguar 5.5*; Schrödinger: Portland, OR, 1991−2003.
(30) Hay, P. J.; Wadt, W. R. *J. Chem. Phys.* **1985**, *82*, 299.
(31) Frisch, M. J.; Trucks, G. W.; Schlegel, H. B.; Scuseria, G. E.; Robb, M. A.; Cheeseman, J. R.; Montgomery, Jr., J. A.; Vreven, T.; Kudin, K. N.; Burant, J. C.; Millam, J. M.; Iyengar, S. S.; Tomasi, J.; Barone, V.; Mennucci, B.; Cossi, M.; Scalmani, G.; Rega, N.; Petersson, G. A.; Nakatsuji, H.; Hada, M.; Ehara, M.; Toyota, K.; Fukuda, R.; Hasegawa, J.; Ishida, M.; Nakajima, T.; Honda, Y.; Kitao, O.; Nakai, H.; Klene, M.; Li, X.; Knox, J. E.; Hratchian, H. P.; Cross, J. B.; Bakken, V.; Adamo, C.; Jaramillo, J.; Gomperts, R.; Stratmann, R. E.; Yazyev, O.; Austin, A. J.; Cammi, R.; Pomelli, C.; Ochterski, J. W.; Ayala, P. Y.; Morokuma, K.; Voth, G. A.; Salvador, P.; Dannenberg, J. J.; Zakrzewski, V. G.; Dapprich, S.; Daniels, A. D.; Strain, M. C.; Farkas, O.; Malick, D. K.; Rabuck, A. D.; Raghavachari, K.; Foresman, J. B.; Ortiz, J. V.; Cui, Q.; Baboul, A. G.; Clifford, S.; Cioslowski, J.; Stefanov, B. B.; Liu, G.; Liashenko, A.; Piskorz, P.; Komaromi, I.; Martin, R. L.; Fox, D. J.; Keith, T.; Al-Laham, M. A.; Peng, C. Y.; Nanayakkara, A.; Challacombe, M.; Gill, P. M. W.; Johnson, B.; Chen, W.; Wong, M. W.; Gonzalez, C.; Pople, J. A. *Gaussian 03*, Revision B.05; Gaussian, Inc., Wallingford CT, 2004.
(32) Marcus, R. A. *J. Chem. Phys.* **1956**, *24*, 966.
(33) Kim, H. J.; Hynes, J. T. *J. Phys. Chem.* **1990**, *94*, 2736.
(34) Gupta, S.; Matyushov D. V. *J. Phys. Chem. A* **2004**, *108*, 2087.
(35) Leontyev, I. V.; Basilevsky, M. V.; Newton, M. D. *Theor. Chem. Acc.* **2004**, *111*, 110.
(36) Tannor, D. J.; Marten, B.; Murphy, R.; Friesner, R. A.; Sitkoff, D.; Nicholls, A.; Ringnalda, M.; Goddard, W. A. III; Honig, B. *J. Am. Chem. Soc.* **1994**, *116*, 11875.
(37) Noodleman, L.; Case, D. A. *Adv. Inorg. Chem.* **1992**, *38*, 423.
(38) Sigfridsson, E.; Olsson, M. H. M.; Ryde, U. *Inorg. Chem.* **2001**, *40*, 2509.
(39) Bearpark, M. J.; Robb, M. A.; Schlegel, H. B. *Chem. Phys. Lett.* **1994**, *223*, 269.
(40) Harvey, J. N.; Aschi, M.; Schwarz, H.; Koch, W. *Theor. Chem. Acc.* **1998**, *99*, 95.
(41) Biesiadka, J.; Loll, B.; Kern, J.; Irrgang K.-D.; Zouni, A.; *Phys. Chem. Chem. Phys.* **2004**, *20*, 4733−4736.
(42) Kamiya, N.; Shen, J.-R. *Proc. Natl. Acad. Sci. U.S.A.* **2003**, *100*, 98−103.
(43) Ferreira, K. N.; Iverson, T. M.; Maghlaoui, K.; Barber, J.; Iwata, S.; *Science* **2004**, *303*, 1831−1838.
(44) Lundberg, M. and Siegbahn, P. E. M.; *Phys. Chem. Chem. Phys.* **2004** *20* 4772−4780.
(45) Creutz, C. *Prog. Inorg. Chem.* **1983**, *30*, 1.
(46) Broo, A.; Larsson, S. *Chem. Phys.* **1992**, *161*, 363.
(47) Ferretti, A.; Lami, A.; Villani, G. *Inorg. Chem.* **1998**, *37*, 2799.
(48) Bencini, A.; Ciofini, I.; Daul, C. A.; Ferretti, A. *J. Am. Chem. Soc.* **1999**, *121*, 11418.
(49) Braun-Sand, S. B.; Wiest, O. *J. Phys. Chem. A* **2003**, *107*, 285.
(50) Vollmer, E.; Kordel, M.; Koslowski, T. *Z. Phys. Chem.* **2004**, *218*, 611.